A digital mapping application for quantifying and displaying air temperatures at high spatiotemporal resolutions in near real-time across Australia

Mathew Webb Corresp., [1] , **Budiman Minasny** [1]

[1] School of Life and Environmental Sciences & Sydney Institute of Agriculture, University of Sydney, Sydney, NSW, Australia

Corresponding Author: Mathew Webb
Email address: mathew.webb@dpipwe.tas.gov.au

Surface air temperature (T_a) required for real-time environmental modelling applications should be spatially quantified to capture the nuances of local-scale climates. This study created near real-time air temperature maps at a high spatial resolution across Australia. This mapping is achieved using the thin plate spline (TPS) interpolation with the help of a digital elevation model and assimilation of 534 telemetered Australian Bureau of Meteorology (BoM) automatic weather station (AWS) sites. The interpolation was assessed using cross-validation analysis in a 1-year period using 30-minute interval observation. This was then applied to an operational real-time mapping of T_a to produce real-time maps at sub-hourly interval via a fully automated mapping system - using the R programming language. The cross-validation analysis revealed root-mean-square errors of 1.6°C, 1.55°C, 1.7°C and 1.74°C for summer, autumn, winter and spring, respectively. On an hourly basis, errors tended to be highest during the late afternoons in spring and summer from 3 pm to 6 pm (AEST), particularly for the coastal areas of Western Australia. The mapping system was capable of regularly providing spatial outputs within 28-minutes of AWS site observations being recorded and had a high degree of temporal reliability. All outputs were displayed in a web mapping application to exemplify a real-time application of the outputs. This study found that the methods employed would be highly suited for similar applications requiring real-time processing and delivery of climate data at high spatiotemporal resolutions across a considerably large land mass.

A digital mapping application for quantifying and displaying air temperatures at high spatiotemporal resolutions in near real-time across Australia

Mathew Webb [1], Budiman Minasny [1]

[1] School of Life and Environmental Sciences & Sydney Institute of Agriculture, The University of Sydney, Eveleigh, NSW, Australia

Corresponding Author:
Mathew Webb [1]
167 Westbury Rd, Prospect, TAS, 7250, Australia
Email address: mathew.webb@dpipwe.tas.gov.au

Abstract

Surface air temperature (T_a) required for real-time environmental modelling applications should be spatially quantified to capture the nuances of local-scale climates. This study created near real-time air temperature maps at a high spatial resolution across Australia. This mapping is achieved using the thin plate spline (TPS) interpolation with the help of a digital elevation model and assimilation of 534 telemetered Australian Bureau of Meteorology (BoM) automatic weather station (AWS) sites. The interpolation was assessed using cross-validation analysis in a 1-year period using 30-minute interval observation. This was then applied to an operational real-time mapping of T_a to produce real-time maps at sub-hourly interval via a fully automated mapping system - using the R programming language. The cross-validation analysis revealed root-mean-square errors of 1.6°C, 1.55°C, 1.7°C and 1.74°C for summer, autumn, winter and spring, respectively. On an hourly basis, errors tended to be highest during the late afternoons in spring and summer from 3 pm to 6 pm (AEST), particularly for the coastal areas of Western Australia. The mapping system was capable of regularly providing spatial outputs within 28-minutes of AWS site observations being recorded and had a high degree of temporal reliability. All outputs were displayed in a web mapping application to exemplify a real-time application of the outputs. This study found that the methods employed would be highly suited for similar applications requiring real-time processing and delivery of climate data at high spatiotemporal resolutions across a considerably large land mass.

Introduction

A timely and accurate source of air temperature (T_a) data is essential for a wide variety of environmental modelling applications requiring real-time monitoring of environmental change (Lazzarini et al. 2014). This is often gleaned from a network of in-situ telemetered meteorological weather stations that are streamed over the internet (Williams et al. 2011). However, such data are only relevant for a single geographic location that fail to accurately account for the spatial variability between sites that can vary markedly over short distances (Webb et al. 2016). For applications that rely on location-specific data, observations are often harvested from stations situated kilometers away from their location of interest, resulting in that data not being truly representative of the desired location (Jeffrey et al. 2001; Liu et al. 2018). This variation is often attributed to the effects of topographic, coastal and latitudinal factors which strongly influence T_a over space (Hutchinson 1991; Jarvis & Stuart 2001a; Wang et al. 2011). As such, T_a for the purpose of input to real-time modelling applications need to be spatially quantified to dynamically account for these interactions but also at an appropriate spatial resolution to account for the subtle nuances of local-scale climates.

There has been a plethora of research aimed at interpolating surface air temperature at various spatiotemporal scales (Hutchinson 1991; Jarvis & Stuart 2001b; Jeffrey et al. 2001; Jones et al. 2009; Xu et al. 2018). This is in addition to surface temperature estimated from satellite data (Mao et al. 2017; Sobrino et al. 2020). Or from regional reanalysis of global circulation models at high spatiotemporal resolutions (Bollmeyer et al. 2015; Su et al. 2019). Despite this, their adoption for real-time monitoring applications have been limited. In the United Arab Emirates, remote sensing data coupled with in-situ meteorological recordings were used to produce sub-hourly air temperature maps in near real-time (Lazzarini et al. 2014). The modelling system produced maps every 15 minutes with the evaluation of the outputs revealing an overall root mean square error average of 2.44°C. The spatial resolution of ~3km, however, is limited in accounting for lapse rates in highly variable topography and would warrant further modification for high-resolution monitoring. Similarly, a near real-time drought monitoring tool developed for South Asia produced daily minimum and maximum temperatures at a spatial resolution of 0.05° (~5km) (Aadhar & Mishra 2017). However, it's application for sub-daily T_a monitoring at the local scale would also require further adaptation. In Australia, the Scientific Information for Land Owners (SILO) database and the Australian Gridded Climate Data (AGCD) interpolate daily minimum (Tmin) and maximum (Tmax) temperatures produced by Australian Bureau of Meteorology (BoM) weather station network to produce maps at 0.05° (~5km) grid resolution (Jeffrey et al. 2001; Jones et al. 2009). Both systems use thin plate smoothing spline (TPS) interpolation to deliver the daily temperature products with an evaluation of the SILO system exhibiting root mean square errors of 1.5°C and 1.9°C for Tmax and Tmin, respectively, and AGCD data showing similar errors of 1.2°C and 1.7°C. Both datasets are available daily with a time lag of 1 day with the SILO predictions accessible via an online platform (www.longpaddock.qld.gov.au/silo). This is used as input to purpose-built applications as demonstrated by the Australian CliMate App (Australian CliMate Development Team 2016). While both datasets are useful for broad-scale analysis requiring up-to-date daily records, they still lacked the resolution for sub-daily real-time monitoring at the local-scale.

Recently, a near-real time mapping system using a combination of regression trees (RT) and TPS interpolation was able to produce spatial products at a spatial resolution of 80m across the state of Tasmania, Australia (Webb et al. 2020). The system was capable of consistently producing maps within an hour of the BoM recordings becoming available. This was further supplemented with the assimilation of 267 non-telemetered logger recording sites; used to enhance interpolation accuracy. Evaluation of the system showed that the TPS method was more suited to real-time application due to the speed and relative accuracy of the outputs produced. Cross-validation assessment showed root mean square errors of 1.42°C, 1.4 °C, 1.34°C and 1.35°C for autumn, winter, spring and summer, respectively, in addition to only requiring 2 minutes processing time to produce each map product. In this context, the application would be suited to the estimation of T_a across a much larger geographic space at a similar spatiotemporal resolution. As such, there is also an opportunity to apply this approach on a digital platform for real-time access for end-users.

The objective of this study was to apply and extend the methods in Webb et al. (2020) for production of T_a maps across continental Australia. TPS interpolation is used to produce T_a maps at sub-hourly intervals (every 30 minutes) based on recordings garnered directly from BoM automatic weather station (AWS) sites. The resulting maps are presented digitally at a spatial resolution of 286m, appropriate for local-scale monitoring purposes. The methods for prediction accuracy are evaluated using historic hourly T_a data captured over a 1-year period, in addition to assessing the efficacy of the system for real-time application and subsequent display of outputs in a purpose-built web mapping application.

Materials & Methods

Approach

The present study consisted of 2 parts. Firstly, evaluation of the TPS methodology using cross-validation; and secondly, application of the methodology for operational real-time mapping of T_a (Fig. 1). For the evaluation purpose of the study, a historical dataset of 30-minute interval T_a recordings was garnered from BoM automatic weather station (AWS) sites for the 1-year period 1 March 2019 to 29 February 2020. This data was used in a leave-one-out cross-validation exercise to assess the prediction performance of the TPS interpolation method. For the application of the methodology for operational real-time mapping, this was tested over a 21-day period from 1 June 2020 to 21 June 2020. For this purpose, a fully automated mapping system was developed using R programming language (R Development Core Team 2015). Processing performance of this mapping system was evaluated for computational efficiency by analyzing each subsequent spatial output (i.e. the time to taken to produce each T_a map) and therefore assessed for real-time application. Maps produced from the interpolation process are immediately displayed in a web map application.

Air temperature (T_a) data

Air temperature (T_a) data recorded by automatic weather stations (AWS) from the Bureau of Meteorology (BoM) and capable of providing real-time access at 30-minute intervals were considered for primary use in this study (Fig. 2). For evaluating the accuracy of the model, a requirement was set, where each station used for the real-time application should have historic recordings for the previous year, specifically from 1 March 2019 to 29 February 2020. These historical data were used for cross-validation analysis. It should be noted that not all AWS sites had data available for the full evaluation period. In these cases, only sites that had least 720 instances of 30-minute interval recordings in each season (15 days) was considered for the evaluation process. AWS sites that did not meet this criterion were discarded from the analysis. Thus, the screening process resulted in 534 AWS sites corresponding to a possible 17567 recording observations in the evaluation period and relevant to each AWS. It should be noted that observations for each AWS site occur 1.2 m above ground using a resistance temperature detector housed in a Stevenson weather screen (Bureau of Meteorology 2018). All AWS recordings are telemetered into the BoM climate database and can be accessed 'live' via the BoM website (e.g. http://www.bom.gov.au/tas/observations/) with most recordings available every half hour with an approximate time lag ranging from 10 min to 20 min from the true observation time.

Interpolating T_a using thin plate smoothing splines (TPS)

T_a values garnered from the BoM AWS sites were interpolated on a 30-minute interval basis using thin plate smoothing splines. This was performed to form TPS predictions in the evaluation period (1 March 2019 to 29 February 2020) as well as for application to real-time mapping. The TPS algorithm was chosen due to its good accuracy for mapping daily minimum and maximum temperatures across Australia (Jeffrey et al. 2001; Jones et al. 2009) and its relative quick computational speed and efficiency (compared to machine learning algorithms) in producing outputs in a timely manner (Webb et al. 2020). Its application involves a trivariate approach whereby latitude, longitude, and elevation variables are used as independent variables, as per Jeffrey et al. (2001). The independent variables of latitude and longitude are used for the partial spline component to account for spatial variation, whereas elevation is combined to account for the temperature lapse rates. The spline component of the algorithm is optimised by minimising the generalized cross validation error from the residual sum of squares (Hutchinson 1991). In this study, the *Fields* statistical package (Nychka et al. 2017) was used to implement the TPS algorithm in R software (R Development Core Team 2015). To guide the mapping of T_a, the 9-second Digital Elevation Model (DEM) was used (Hutchinson et al. 2008). This was reprojected to Geocentric Datum of Australia 94, Geoscience Australia Lambert projection; and resampled to a spatial resolution of 286 m (roughly equivalent to the spatial resolution of original 9-second

DEM). The geographical coordinates of the AWS site locations were then spatially intersected with the newly resampled DEM. This operation provided a consistent template to routinely form TPS models using the AWS observations as data points to the algorithm (on a half-hourly basis). Thus, T_a predictions generated by each TPS model were spatially interpolated using the DEM as the z variable, along with the coordinate parameters of the inherent cell properties of the DEM acting as the latitude (x) and longitude (y) variables. This allowed the spline smoothing parameter to be applied continuously across the geographic feature space of the DEM, resulting in a final mapped prediction; saved as GeoTIFF rasters.

Evaluating TPS interpolation

The performance of the TPS algorithm was evaluated in the period from 1 March 2019 to 29 February 2020. A leave-one-out cross-validation procedure was employed for each AWS site, whereby the training dataset was split into i parts such that i is equal to the number of AWS sites, i.e. 534. For each AWS in i, the i^{th} AWS site was kept for validation (i.e. using actual recordings from the evaluation period), while the remaining dataset, comprising of the remaining BoM recordings was used for TPS modelling to predict T_a at the i^{th} AWS site. This was performed for each 30-minute interval (h) in the evaluation period to produce a set of modelled TPS estimates versus actual AWS recordings at each site. This equated to 17,567 modelled TPS predictions where actual observations from each AWS site could then be compared. Validation metrics used to assess the modelling accuracy included the mean absolute error (MAE), root-mean-square error (RMSE), coefficient of determination (R^2) and the concordance coefficient. The concordance coefficient (p_c) was used to assess agreement between TPS predictions x; and actual recordings y; that fall on the 45° line through the origin, as defined by Lin (1989):

$$p_c = \frac{2p\sigma_x\sigma_y}{\sigma_x^2 + \sigma_y^2 + (\mu_x - \mu_x)^2}$$

where for μ_x and μ_x represent the means for x and y, respectively, σ_x^2 and σ_y^2 represent the corresponding variances, and p is the correlation coefficient between x and y. A concordance rating close to one indicates strong agreement between predicted and actual T_a pairings that fall on the 45° line through the origin.

Application to real-time monitoring of T_a

The proposed methodology was assessed for operational real-time monitoring of T_a by automating the process using software R (R Development Core Team 2015), thereby developing a fully automated mapping system. The system was trialled over a 21-day period from 1 June 2020 to 21 June 2020, using 'real-time' BoM observations to drive the system. The program consisted of two components, firstly the import of live T_a data via the internet from the BoM website, and secondly, the mapping of the observations using TPS interpolation. For the live BoM observations, these were automatically downloaded for individual station observations every 30-minutes from the BoM observations portal (e.g. http://www.bom.gov.au/fwo/IDT60801/IDT60801.<*stationIDnumber*>.axf). These data were accessed as a comma delimited text file which was routinely updated every 30 minutes with an approximate time lag ranging from 5 to 20 minutes from when the observation was recorded (observation updates varied from station to station). The mapping system was programmed to query and import recordings every 30-minutes (bi-hourly) that corresponded to the nearest half-hour at 0 and 30 minutes (past the hour). Because of the observational time lags, the system was programmed to make queries at 5, 10, 15, 20, 25 and 30 minutes within their 30-minute processing window. Also, a threshold was set where at least 480 out of the 534 BoM stations (i.e. 90% of total available AWS sites that were used in the evaluation analysis) have available observations before the mapping was allowed to commence at their respective processing times. This serves to instil integrity into the system and thereby limit the number of missing observations that could otherwise produce inaccuracies into the final mapped output. However, if this threshold was not met during the query times, the mapping was still permitted to commence at the 30-minute mark regardless of the number of observations available (this was subsequently recorded). All AWS recording times were standardised to Australian Eastern Standard Time (AEST).

To interpolate the TPS predictions, the Raster package (Hijmans & van Etten 2012) in combination with the *Fields* statistical package (Nychka et al. 2017) was used to map the predictions in a continuous manner across Australia. To improve processing speed, the clusterR function within the Raster package was parameterised to host the TPS algorithm, thereby enabling mapping to occur using multi-core processors. In this manner, the mapping system was hosted on a high-end cloud computing Linux platform (Ubuntu 18.04 LTS (Bionic)) constituting 16 virtual CPU cores and 64GB RAM; made available courtesy of the Australian National eResearch Collaboration Tools and Resources project (NeCTAR). Spatial outputs were saved as individual GeoTIFF raster format at a grid cell resolution of 286m, i.e. equivalent to the spatial resolution of the resampled DEM.

Results

Assessment of the TPS interpolation procedure

Each of the AWS sites underwent the leave-one-out cross-validation analysis to assess TPS prediction accuracy for T_a in the evaluation period: 1 March 2019 to 29 February 2020. This analysis revealed broad similarities across the seasons with MAE values ranging between 1.16°C in autumn to 1.29°C in spring, and RMSE ranging between 1.55°C to 1.74°C for autumn and spring, respectively (Table 1). The R^2 and P_c values were above 0.8 indicating that the TPS predictions were strongly correlated to the validation data in addition to being highly associated with the 45° line through the origin (Lin 1989). This assessment also implied that predictions were relatively consistent across the evaluation period and did not vary substantially on a seasonal basis. Moreover, it was clear that the TPS interpolation was more suited to predicting T_a

in autumn which exhibited superior statistics across all validation measures when compared to the other seasons. However, TPS predictions tended to be least accurate in spring which had MAE and RMSE values that was greater by 0.13°C and 0.19°C, respectively, when compared to the corresponding MAE and RMSE values in autumn. Interestingly, although spring exhibited comparatively inferior MAE and RMSE values, the R^2 statistics were similar, both registering 0.91. This suggests that while errors were comparatively larger in spring, they were still very highly correlated to the validation data. However, it should be noted that the coefficient of determination may have been unrealistically overestimated for spring since the seasonal data signal was not removed prior to analysis, as advocated in Jeffrey et al. (2001).

When looking at the histogram distribution of the MAE it was apparent that spring and winter had a large proportion of AWS sites that exhibited MAE values above 2°C (Fig. 3). This contributed to the inflated error values shown in Table 1. Specifically, spring and winter both had a total of 42 and 46 AWS sites that registered MAE above 2°C compared to 22 and 16 AWS sites for summer and autumn, respectively.

When viewing these errors spatially, it was clear that the majority of the larger interpolation errors transpired in regions where there was a lack of neighbouring AWS sites (Fig. 4). Specifically, the central and western interior parts of Australia tended to exhibit MAE values above 2°C, compared to the eastern half where temperatures were consistently predicted within 1.5°C of the actual T_a. Of particular note was the predominately high errors encountered for the coastal areas of Western Australia (between Geraldton and Port Hedland) during summer and spring where prediction errors were regularly above 2.5°C. For example, the Learmonth Airport AWS site (Fig. 2) had MAE of 3.4°C and 3.15°C for spring and summer, respectively. Outside of this cluster, there were also high MAE values for individual AWS sites located at Pirlangimpi Airport (Tiwi Islands, Northern Territory) with MAE of 3.57°C in spring; Forrest in Western Australia with MAE of 2.86°C in summer; and Yampi Sound in Northern Territory with MAE of 3.27°C in winter. Furthermore, in winter there was a notable cluster of high MAE values emanating from central Australia through to the coastal fringes of Northern Territory and Western Australia (i.e. Darwin through to Broome) with MAE consistently above 2°C.

When observing MAE values over a 24-hour period (Fig. 5), it was clear that the high MAE values encountered for the coastal areas of Western Australia in summer and spring tended to occur during afternoons. Specifically, these had MAE ranging between 4-6°C for times 3 pm to 6 pm, i.e. 1 pm to 4 pm, Australian Western Standard Time (AWST). Of particular note was the Learmonth Airport AWS site registering MAE of 6.88°C, peaking at 5 pm (3 pm, AWST) in summer (Fig. 6). Similarly, very high MAE values were encountered for the south-eastern area of Western Australia, notably for the Forrest AWS site at 6 pm, which registered MAE of 6.07°C and 5.25°C for spring and summer, respectively (Fig. 6). This was in addition to the Ceduna AWS site (South Australia) at 6 pm, which registered a MAE of 5.41°C in summer. During winter the trend for high MAE in central Australia and the coastal fringes of Northern Territory and Western Australia tended to occur during early mornings from 3 am to 9 am (1 am to 7 am, AWST), with MAE ranging from 3-5°C. The AWS sites with the greatest MAE in these parts were Adele Island and Yampi Sound which exhibited values of 6.41°C and 6.4°C, respectively, at 8 am (Fig. 6). Both sites are located in the northern coastal region of Western Australia (NB: the locations of all aforementioned AWS sites are depicted in Fig. 2).

Assessment of mapping T_a in near real-time

The TPS methodology was applied to mapping T_a in real-time at 30-minute intervals over a 21-day period from 1 June 2020 to 21 June 2020. This exercise resulted in 1007 maps being produced which aligned to the total number of 30-minute processing intervals in the trial period; confirming all possible maps were successfully processed. On analysing the map completion times, the majority of the maps were completed at 28 minutes (Fig. 7). Specifically, 410 and 414 maps were produced for their respective 0- and 30-minute processing intervals. This corresponded directly to the AWS import times (Fig. 8), with the same proportion of AWS observations reaching the 480-observation threshold import limit at the 15-minute mark; thereby permitting T_a mapping to commence. Thus, import times that occurred at 15-minutes, equated to resulting maps being completed at 28-minutes from the AWS observation time. From this, it can be deduced that on all occasions the map processing time was 13-minutes, regardless of the interval being processed. It should be noted that on 35 occasions the 480-observation threshold limit was not reached, resulting in maps - that did not meet this criterion - being produced at the 30-minute mark. This equated to 14 and 21 maps produced at the 0- and 30-minute processing intervals, respectively.

Discussion

Appraisal of the TPS interpolation procedure

On the whole, the TPS interpolation method was a reliable predictor of T_a across Australia with an average the RMSE of 1.65°C (i.e. when averaged across the seasons in Table 1). When compared to previous studies, this error was similar to Jeffrey et al. (2001) with RMSE of 1.5°C and 1.9°C for daily maximum and minimum temperatures, respectively; and Jones et al. (2009) with corresponding RMSE of 1.2°C and 1.7°C. On a seasonal basis the TPS predictions tended to be least accurate in spring which had MAE and RMSE values larger by 0.13°C and 0.19°C, respectively, compared to the same measures in autumn. When viewing these errors spatially, it was clear that the majority of the larger interpolation errors transpired in the central and western interior parts of Australia. This is unsurprising given the station density in these parts are relatively sparse in addition to large temperature variances which tend to produce inflated errors (Jeffrey et al. 2001; Jones & Trewin 2000). Of particular note was the predominately high errors encountered for the coastal areas of Western Australia (between Geraldton and Port Hedland) during summer and spring where prediction errors were regularly above 2.5°C. This was in addition to high MAE values for individual AWS sites located at Forrest in Western Australia and Ceduna in South Australia. Collectively, these regions tend to experience very strong gradients for maximum temperatures due to their proximity between the coast and inland deserts regions (Jones et al. 2009). These are invariably difficult to model with a sparse network of observation sites since these errors are amplified during mid to late afternoons in late spring and summer when the temperature gradients were at their greatest. Also, temperatures in these areas can vary considerably over short periods leading to a tendency for larger errors (Jones & Trewin 2000). Concerning winter, the trend for high MAE in central Australia and coastal fringes of Northern Territory and Western Australia tended to occur during early mornings from 3 am to 9 am (1 am to 7 am, AWST). As acknowledged previously, the accuracy of the mapping was limited in these regions due to an insufficient network of AWS sites. Also, AWS sites in the coastal fringes tend to have tight climate gradients as a result of local maritime effects (Jones et al. 2009). Thus, the sparse network of AWS sites would not be able to account for these on a sub-hourly timescale. Moreover, the spread of AWS sites in remote coastal locations – e.g. Adele Island, Yampi Sound and Pirlangimpi Airport AWS sites - tend to have considerably larger errors as a result of unique and often complex microclimates (Jones et al. 2009). It should also be noted that the larger errors for the central interior parts of Australia may also be due to the weaker link between altitude and minimum temperature – for which the TPS algorithm is reliant (Hutchinson 1991). This is because minimum temperatures have a highly variable and complex relationship with topography for which elevation and its association with lapse rates are only one part (Rolland 2003; Trewin 2005). Considering minimum temperatures tend to transpire during early mornings – as encountered for AWS sites in winter (Fig. 5 & 6) – a multivariate approach to modelling might be more appropriate along with a denser network of AWS sites. This approach was conducted by Webb et al. (2020) that showed errors improved during winter when using regression tree interpolation over TPS. However, the substantially longer processing times may not be appropriate for real-time application, negating its ability to produce outputs in a timely manner as required for this study.

It should be commented that the cross-validation analysis adopted in this study would likely overestimate the error since predictions made at locations have actual data observations. This would be less of a concern for regions where the number of observation points is numerous, such as for the majority of land areas in south-east Australia – which tended to have more accurate T_a predictions compared to the western interior. Nevertheless, this exemplifies that the sparse network of AWS sites in central and western coastal areas of Australia was a notable factor contributing to larger interpolation errors.

Appraisal of mapping T_a in near real-time and application to digital mapping

The TPS interpolation applied in real-time was capable of producing sub-hourly T_a maps typically within 28-minutes of the observation being recorded by the available AWS sites (Fig. 7). Specifically, import times were generally reached for the predefined threshold of 480 observations at the 15-minute mark (Fig. 8) which was followed by a 13-minute processing lag.

In this regard, maps were consistently available within their 30-minute processing window and had a high degree of temporal reliability - with all possible maps produced in the 21-day trial period. The resulting maps were presented on a digital web mapping platform to allow real-time access and interrogation ability of each output. An example of this application can be accessed at URL http://austemperature.live/ (Fig. 9). A GeoServer backend was used to host current outputs to allow geospatial representation and sharing of outputs via a Wep Map Service (Open Source Geospatial Foundation 2019). The maps can be spatially queried to reveal temperatures for the current hour and also for the previous 3-hrs (at 30-minute intervals). This is enabled via web application packages *shiny* and *leaflet* (Chang et al. 2019; Cheng et al. 2019) within the R programming environment (R Development Core Team 2015). In this fashion, maps can be spatially interrogated via an on-the-fly 'data drilling' for any geographical location in Australia (via mouse click). A facility to view the cross-validation statistics of each map output is also provided as well as the ability to download each newly created map for use in GIS applications. Rainfall mapping outputs are also presented, although this should be used with caution due to the preliminary nature of this work.

Conclusions

The methods described in this study were successful for operational real-time spatial mapping of T_a at high spatiotemporal across Australia. The TPS interpolation method was best suited for mapping T_a during autumn and was comparatively less accurate during winter and spring. In particular, areas, where there was a lack of AWS sites, tended to underperform. These areas included the central and western interior regions of Australia, as well for the north-west coastal areas of Western Australia. On a temporal basis, the errors were amplified during the afternoons, particularly around the coastal regions of Western Australia, during spring and summer. In winter, errors tended to be higher in central Australia and the coastal fringes of Northern Territory and Western Australia, from 3 am to 9 am. In terms of applying the TPS method to real-time operational mapping, the mapping system was able to regularly provide spatial outputs within 28-minutes of AWS site observations being recorded. In addition, it also had a high degree of temporal reliability with all maps produced in the 21-day trial period. Outputs were sequentially displayed on purpose-built web mapping application to exemplify real-time application of the outputs. In this regard, the methodology employed in this study would be highly suited for similar applications requiring real-time processing and delivery of climate data at high spatiotemporal resolutions across a large landmass, suitably complimented with a relatively dense network of observation sites.

Acknowledgements

This research was supported by Tasmanian Partnership for Advanced Computing and by use of the Nectar Research Cloud. The Nectar Research Cloud is a collaborative Australian research platform supported by the National Collaborative Research Infrastructure Strategy (NCRIS).Add your acknowledgements here.

References

Aadhar S, and Mishra V. 2017. High-resolution near real-time drought monitoring in South Asia. *Scientific Data* 4:170145. 10.1038/sdata.2017.145

Australian CliMate Development Team. 2016. Australian CliMate: Climate analysis for decision makers. University of Southern Queensland, Australia. https://climateapp.net.au/.

Bollmeyer C, Keller JD, Ohlwein C, Wahl S, Crewell S, Friederichs P, Hense A, Keune J, Kneifel S, Pscheidt I, Redl S, and Steinke S. 2015. Towards a high-resolution regional reanalysis for the European CORDEX domain. *Quarterly Journal of the Royal Meteorological Society* 141:1-15. 10.1002/qj.2486

Bureau of Meteorology. 2018. Bureau of Meteorology website. (Australian Government). *Available at http://www.bom.gov.au/climate/cdo/about/airtemp-measure.shtml* (accessed 11 August.

Chang W, Cheng J, Allaire J, Xie Y, and McPherson J. 2019. shiny: Web Application Framework for R. R package version 1.4.0. https://CRAN.R-project.org/package=shiny.

Cheng J, Karambelkar B, and Xie Y. 2019. leaflet: Create Interactive Web Maps with the JavaScript 'Leaflet' Library. R package version 2.0.3. https://CRAN.R-project.org/package=leaflet.

Hijmans RJ, and van Etten J. 2012. raster: Geographic analysis and modeling with raster data. R package version 2.0-12. http://CRAN.R-project.org/package=raster.

Hutchinson M. 1991. The application of thin plate smoothing splines to continent-wide data assimilation. In: Jasper J, editor. Data Assimilation Systems. Melbourne, Vic, Australia: Bureau of Meteorology. p 104-113.

Hutchinson MF, Stein JL, Stein JA, Anderson H, and Tickle PK. 2008. GEODATA 9 second DEM and D8: Digital Elevation Model Version 3 and Flow Direction Grid. Record DEM-9S.v3. Geoscience Australia, Canberra.

Jarvis CH, and Stuart N. 2001a. A comparison among strategies for interpolating maximum and minimum daily air temperatures. Part I: The selection of "guiding" topographic and land cover variables. *Journal of Applied Meteorology* 40:1060-1074.

Jarvis CH, and Stuart N. 2001b. A comparison among strategies for interpolating maximum and minimum daily air temperatures. Part II: The interaction between number of guiding variables and the type of interpolation method. *Journal of Applied Meteorology* 40:1075-1084.

Jeffrey SJ, Carter JO, Moodie KB, and Beswick AR. 2001. Using spatial interpolation to construct a comprehensive archive of Australian climate data. *Environmental Modelling & Software* 16:309-330. https://doi.org/10.1016/S1364-8152(01)00008-1

Jones DA, and Trewin BC. 2000. On the relationships between the El Niño–Southern Oscillation and Australian land surface temperature. *International journal of climatology* 20:697-719. 10.1002/1097-0088(20000615)20:7<697::aid-joc499>3.0.co;2-a

Jones DA, Wang W, and Fawcett R. 2009. High-quality spatial climate data-sets for Australia. *Australian Meteorological and Oceanographic Journal* 58:233.

Lazzarini M, Marpu PR, Eissa Y, and Ghedira H. 2014. Toward a Near Real-Time Product of Air Temperature Maps from Satellite Data and In Situ Measurements in Arid Environments. *IEEE Journal of Selected Topics in Applied Earth Observations and Remote Sensing* 7:3093-3104. 10.1109/JSTARS.2014.2320762

Lin LIK. 1989. A Concordance Correlation Coefficient to Evaluate Reproducibility. *Biometrics* 45:255-268. 10.2307/2532051

Liu S, Su H, Tian J, and Wang W. 2018. An analysis of spatial representativeness of air temperature monitoring stations. *Theoretical and Applied Climatology* 132:857-865. 10.1007/s00704-017-2133-6

Mao KB, Ma Y, Tan XL, Shen XY, Liu G, Li ZL, Chen JM, and Xia L. 2017. Global surface temperature change analysis based on MODIS data in recent twelve years. *Advances in Space Research* 59:503-512. https://doi.org/10.1016/j.asr.2016.11.007

Nychka D, Furrer R, Paige J, and Sain S. 2017. fields: Tools for spatial data. R package version 10.3. https://github.com/NCAR/Fields.

Open Source Geospatial Foundation. 2019. Geoserver: an open source software server for sharing and editing geospatial data. GeoServer 2.17.1. http://geoserver.org/release/stable/.

R Development Core Team. 2015. R: A language and environment for statistical computing. R Foundation for Statistical Computing. Vienna, Austria.

Rolland C. 2003. Spatial and Seasonal Variations of Air Temperature Lapse Rates in Alpine Regions. *Journal of Climate* 16:1032-1046. 10.1175/1520-0442(2003)016<1032:sasvoa>2.0.co;2

Sobrino J, Julien Y, and García-Monteiro S. 2020. Surface Temperature of the Planet Earth from Satellite Data. *Remote Sensing* 12:218. 10.3390/rs12020218

Su CH, Eizenberg N, Steinle P, Jakob D, Fox-Hughes P, White CJ, Rennie S, Franklin C, Dharssi I, and Zhu H. 2019. BARRA v1.0: the Bureau of Meteorology Atmospheric high-resolution Regional Reanalysis for Australia. *Geosci Model Dev* 12:2049-2068. 10.5194/gmd-12-2049-2019

Trewin BC. 2005. A notable frost hollow at Coonabarabran, New South Wales. *Australian Meteorological Magazine* 54:15-21.

Wang K, Sun J, Cheng G, and Jiang H. 2011. Effect of altitude and latitude on surface air temperature across the Qinghai-Tibet Plateau. *Journal of Mountain Science* 8:808-816. 10.1007/s11629-011-1090-2

Webb M, Hall A, Kidd D, and Minasny B. 2016. Local-scale spatial modelling for interpolating climatic temperature variables to predict agricultural plant suitability. *Theoretical and Applied Climatology* 124:1145-1165. 10.1007/s00704-015-1461-7

Webb MA, Kidd D, and Minasny B. 2020. Near real-time mapping of air temperature at high spatiotemporal resolutions in Tasmania, Australia. *Theoretical and Applied Climatology*. 10.1007/s00704-020-03259-4

Williams M, Cornford D, Bastin L, Jones R, and Parker S. 2011. Automatic processing, quality assurance and serving of real-time weather data. *Computers & Geosciences* 37:353-362. https://doi.org/10.1016/j.cageo.2010.05.010

Xu Y, Knudby A, Shen Y, and Liu Y. 2018. Mapping Monthly Air Temperature in the Tibetan Plateau From MODIS Data Based on Machine Learning Methods. *IEEE Journal of Selected Topics in Applied Earth Observations and Remote Sensing* 11:345-354. 10.1109/JSTARS.2017.2787191

Figure 1

Workflow developed for this study

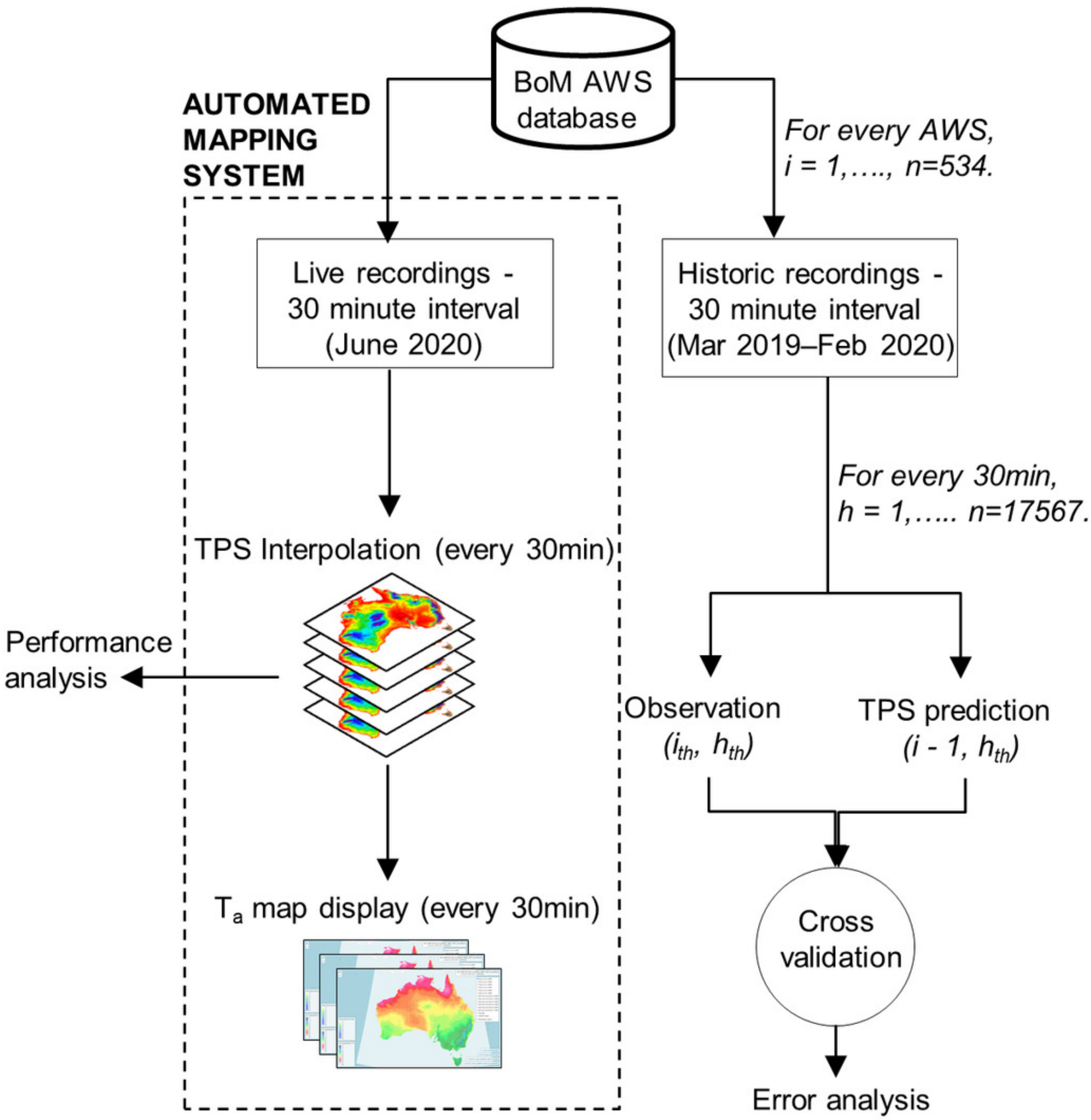

Figure 2

Elevation map of Australia with locations of major towns/cities and Bureau of Meteorology (BoM) automatic weather stations (AWS).

Purple dots illustrate AWS locations. Red dots denote locations of notable AWS sites (refer results section)

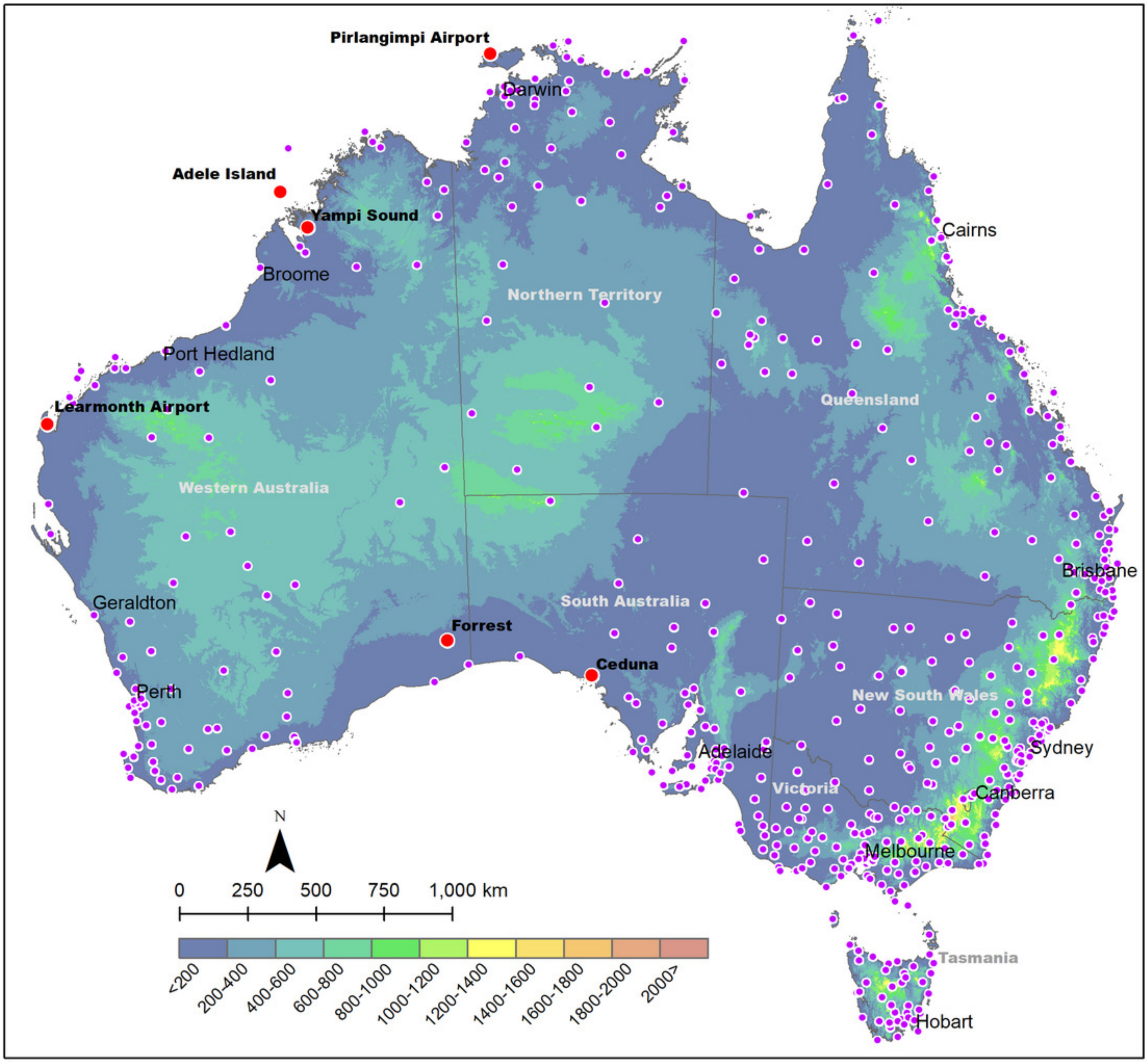

Figure 3

Histogram plots of MAE values in each season with fitted cumulative frequency curves.

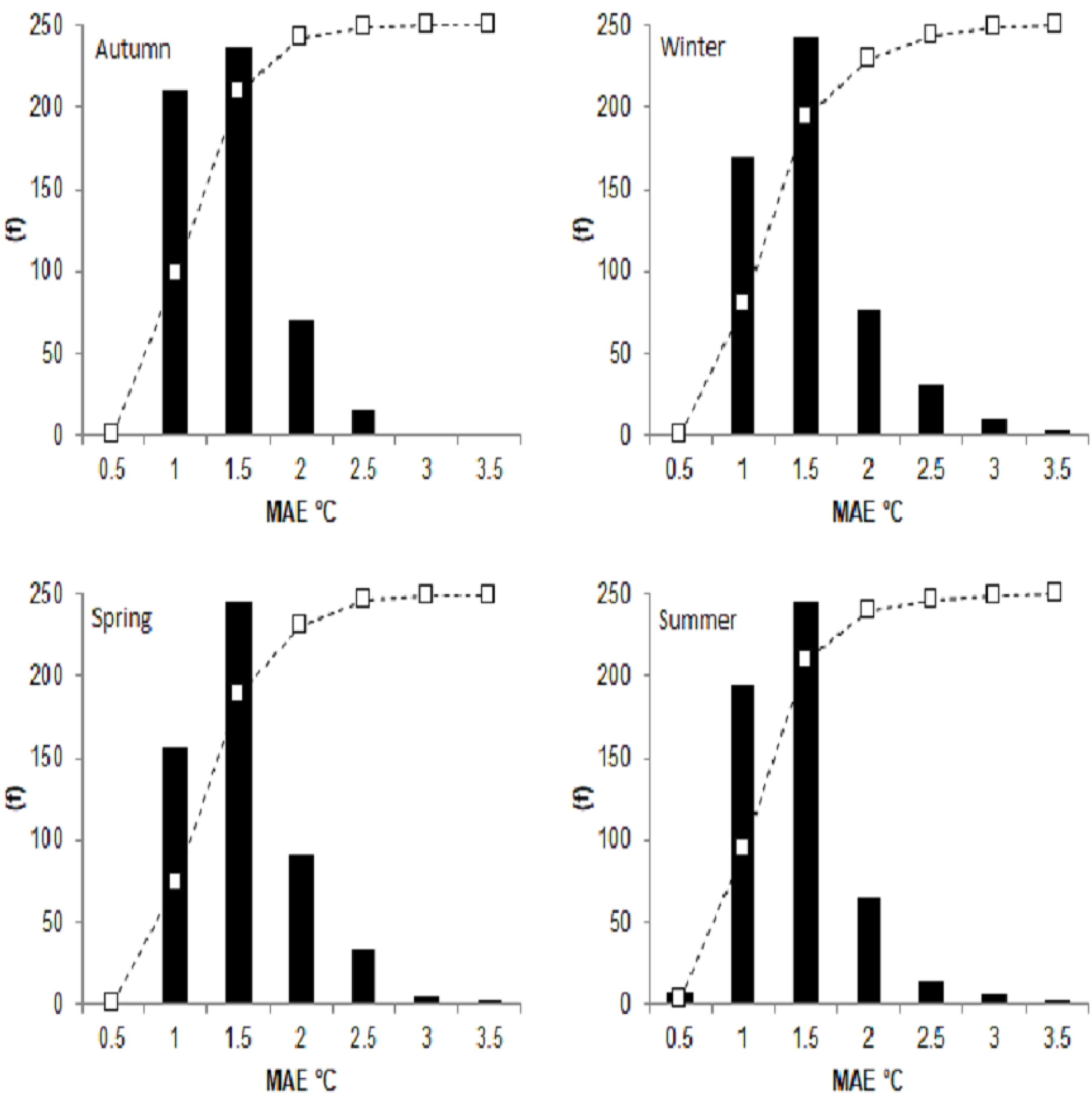

Figure 4

Interpolated MAE °C values (using a two-dimensional smoothing spline) produced from individual AWS sites in each season.

Black dots illustrate locations of AWS sites. Larger dots denote AWS sites where MAE values are above the 95th percentile (labelled with their corresponding MAE value).

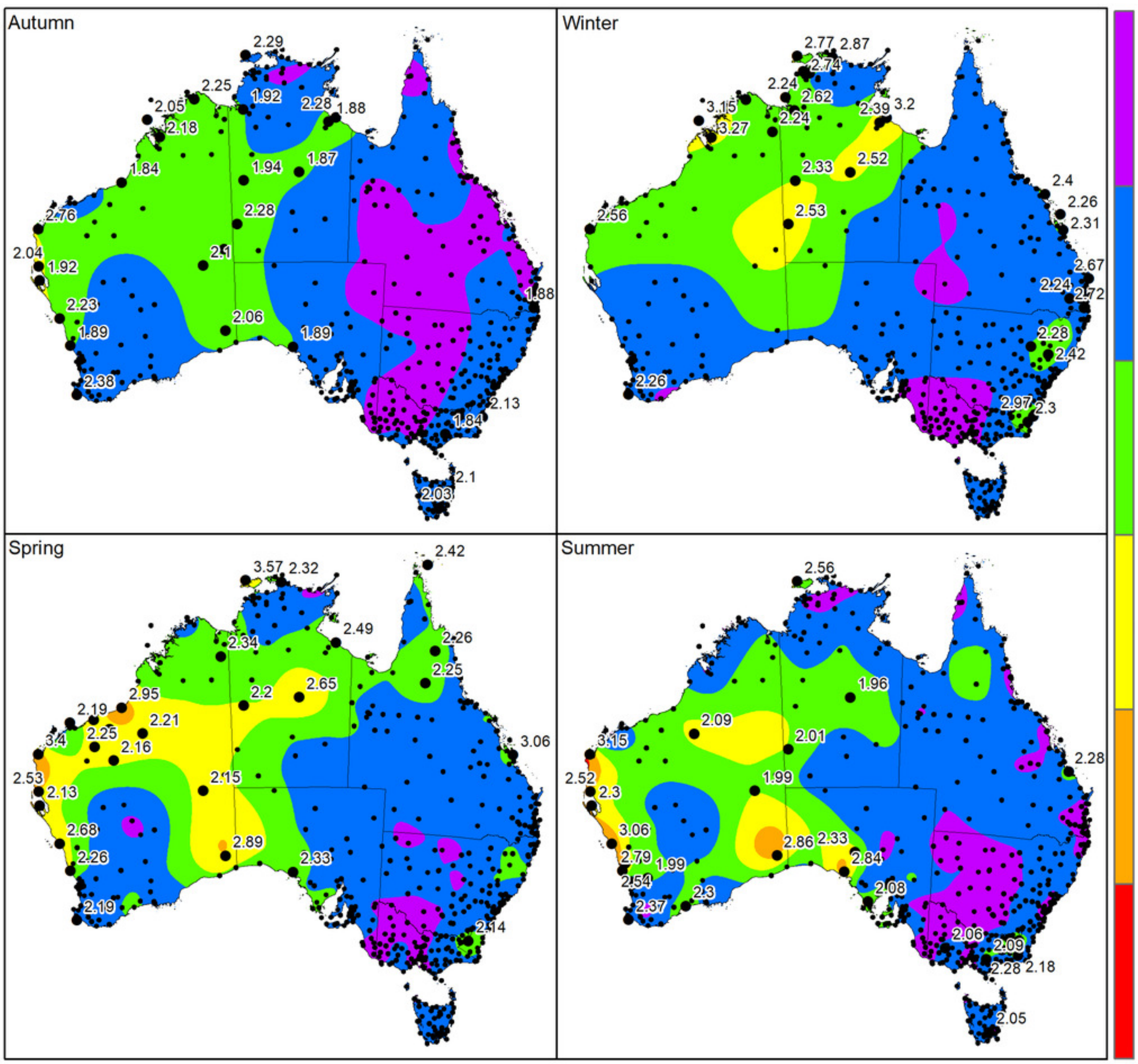

Figure 5

Interpolated MAE °C values (using a two-dimensional smoothing spline) for the 24-hour period in each season. Maps are displayed at 3-hourly intervals for times 12am, 3am, 6am, 9am, 12pm, 3pm, 6pm and 9pm (AEST).

Aut Autumn, Win Winter, Spr Spring, Sum Summer

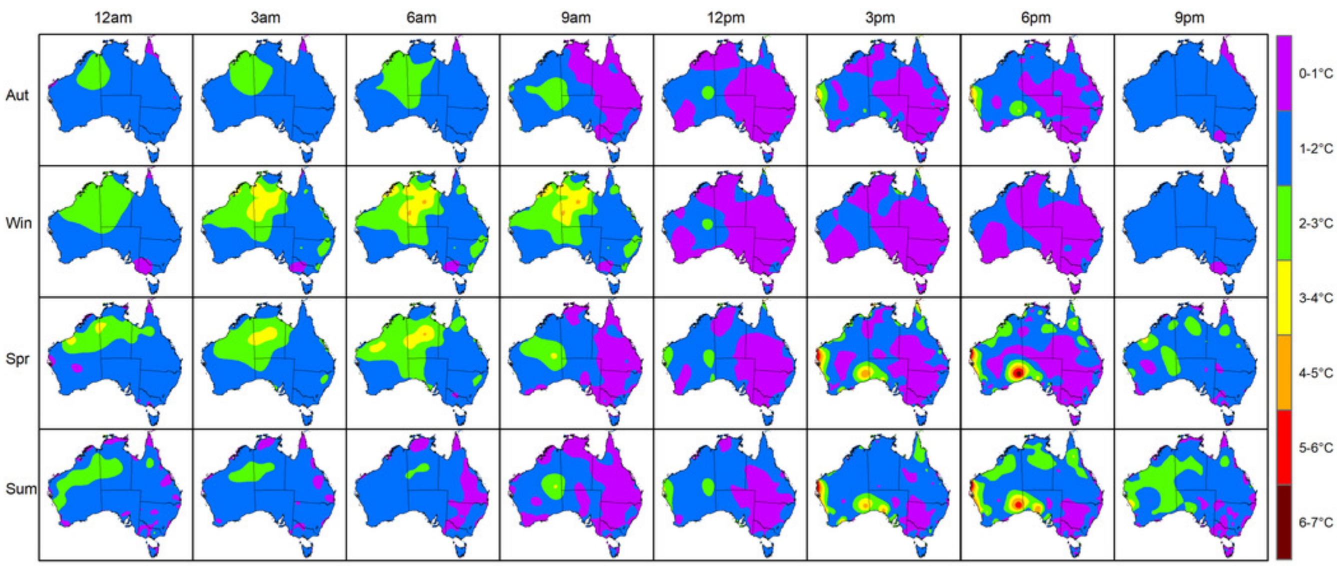

Figure 6

Mean absolute error (MAE, °C) over a 24-hour period (AEST) averaged for selected AWS site in each season.

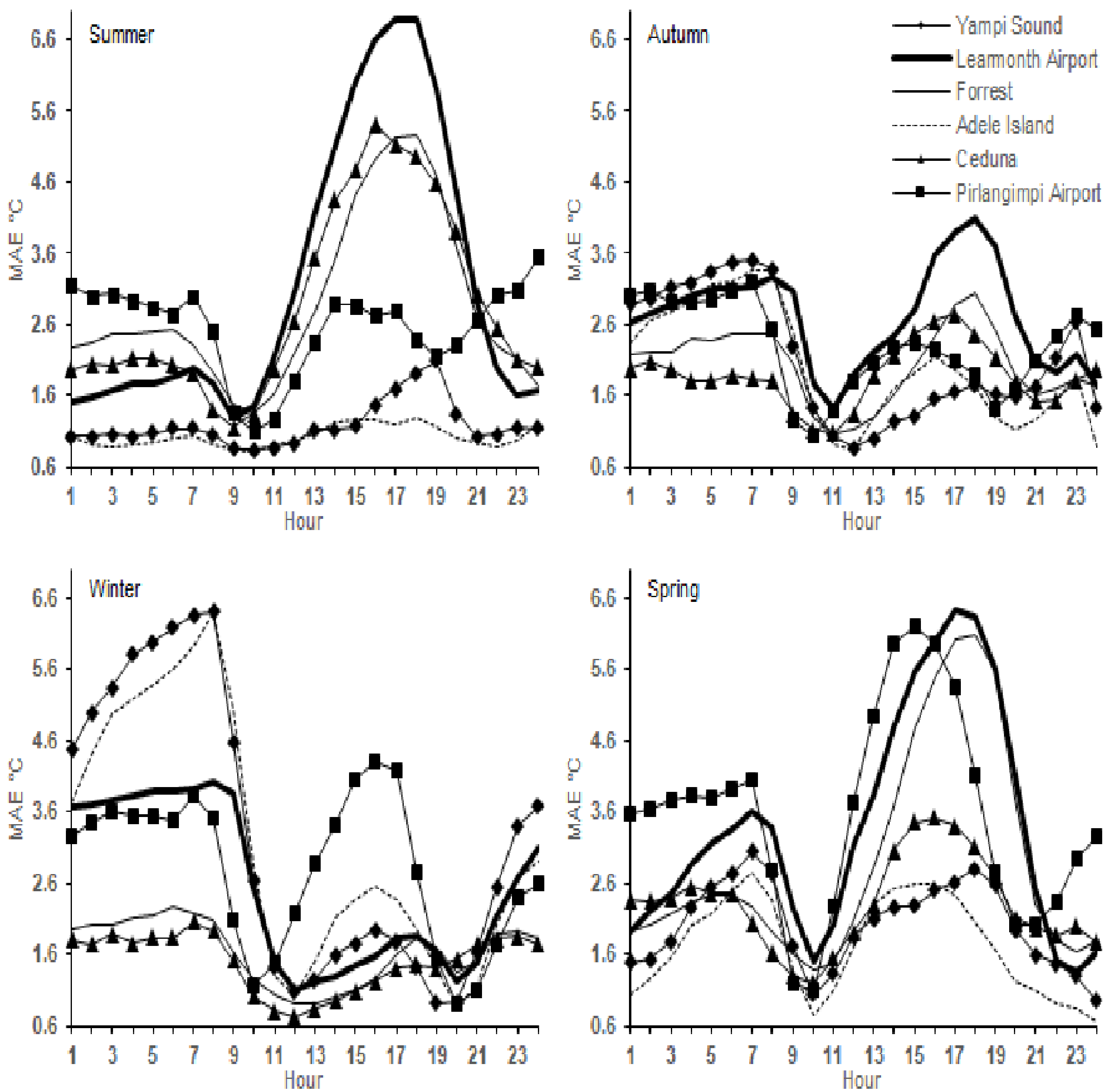

Figure 7

Frequency of map completion times (minutes from AWS observation time, T) in accordance to their bi-hourly processing intervals at 0 (a) and 30 (b) minutes.

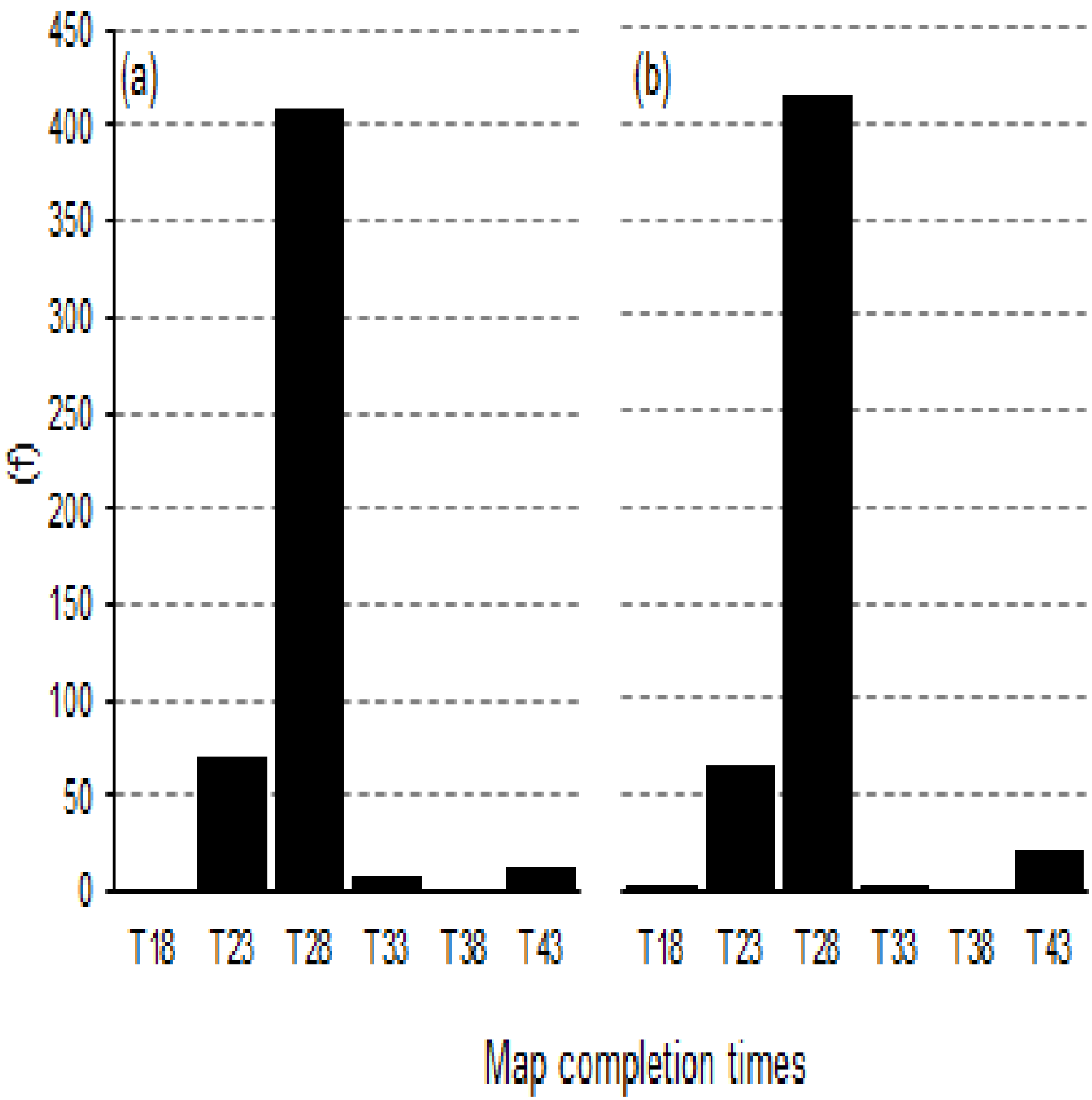

Figure 8

Box and whisker plots for AWS import times (minutes from AWS observation time, T) in accordance to their bi-hourly processing intervals at 0 (a) and 30 (b) minutes.

Numbers in bold denote frequencies when the 480-observation threshold limit was reached.

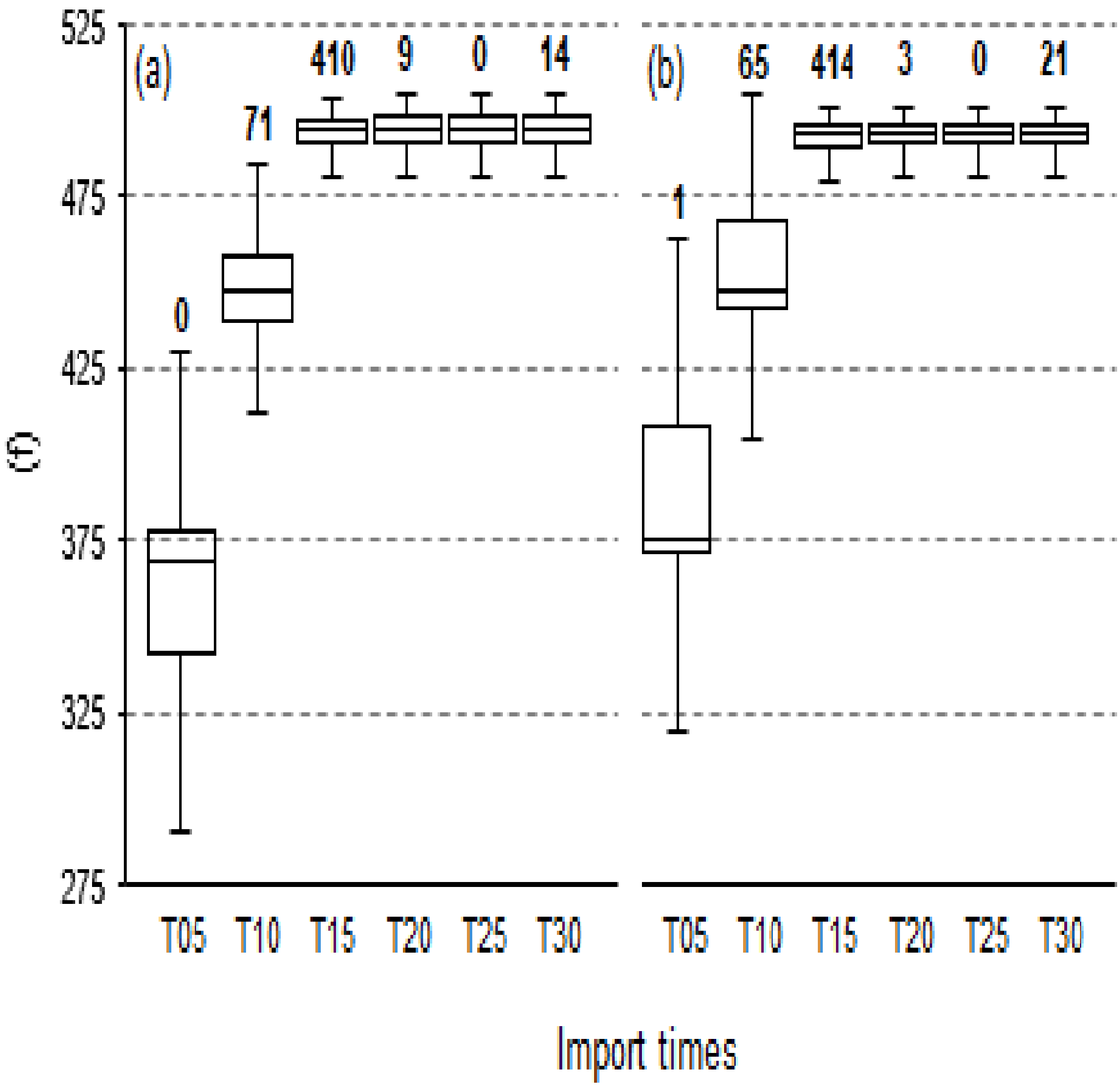
525
475
425
375
325
275
(f)
(a)
0
71
410
9
0
14
(b)
1
65
414
3
0
21
T05
T10
T15
T20
T25
T30
T05
T10
T15
T20
T25
T30
Import times

Figure 9

Web map environment for displaying and spatially interrogating the near real-time Ta outputs. An example can be viewed at URL http://austemperature.live/.

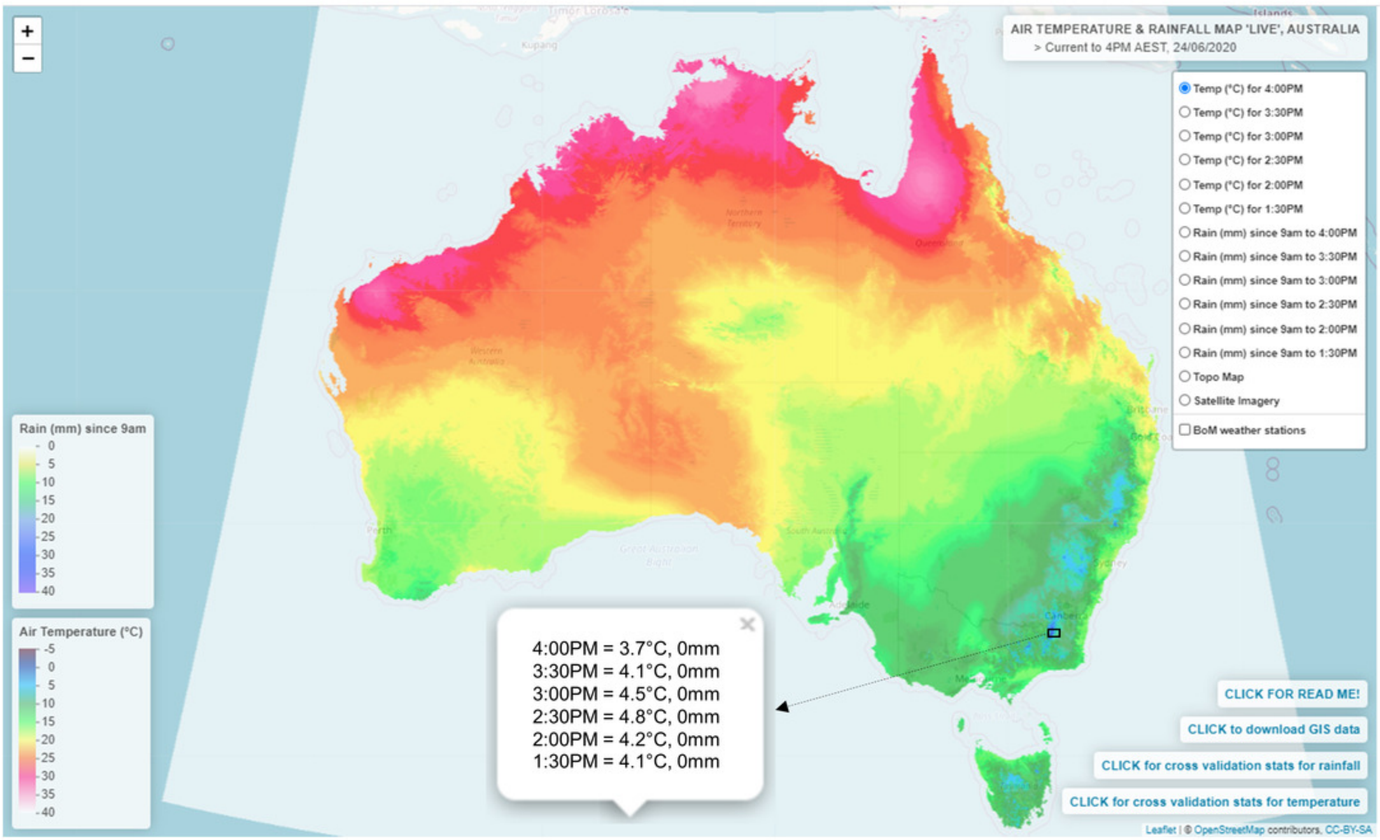

Table 1(on next page)

Validation statistics for the TPS interpolation procedure showing the coefficient of determination (R^2), concordance coefficient (P_c), mean absolute error (MAE, °C) and root-mean-square error (RMSE, °C) averaged for each

sd standard deviation, min minimum, max maximum

	Summer	Autumn	Winter	Spring
R^2				
mean	0.89	0.91	0.86	0.91
min	0.05	0.02	0.01	0.01
max	0.99	0.99	0.97	0.99
sd	0.11	0.09	0.11	0.09
P_c				
mean	0.92	0.94	0.92	0.93
min	0.18	0.14	0.18	0.09
max	0.99	0.99	0.99	0.99
sd	0.09	0.08	0.09	0.08
MAE				
mean	1.17	1.16	1.27	1.29
min	0.45	0.48	0.52	0.57
max	3.15	2.76	3.27	3.57
sd	0.41	0.36	0.47	0.45
RMSE				
mean	1.6	1.55	1.7	1.74
min	0.62	0.67	0.74	0.77
max	4.25	3.49	4.26	4.31
sd	0.54	0.47	0.61	0.57

1